Guenther Carlos Krieger
guenther@usp.br

Jurandir Itizo Yanagihara
jiy@usp.br
Department of Mechanical Engineering (PME)
Escola Politécnica – University of São Paulo
055809-900 São Paulo, SP, Brazil

Prediction of the Temperature Distribution of Partially Submersed Umbilical Cables

The objective of this work is to predict the temperature distribution of partially submersed umbilical cables under different operating and environmental conditions. The commercial code Fluent® was used to simulate the heat transfer and the air fluid flow of part of a vertical umbilical cable near the air-water interface. A free-convective three-dimensional turbulent flow in open-ended vertical annuli was solved. The influence of parameters such as the heat dissipating rate, wind velocity, air temperature and solar radiation was analyzed. The influence of the presence of a radiation shield consisting of a partially submersed cylindrical steel tube was also considered. The air flow and the buoyancy-driven convective heat transfer in the annular region between the steel tube and the umbilical cable were calculated using the standard k-ε turbulence model. The radiative heat transfer between the umbilical external surface and the radiation shield was calculated using the Discrete Ordinates model. The results indicate that the influence of a hot environment and intense solar radiation may affect the umbilical cable performance in its dry portion.

Keywords: *umbilical cable, conjugate heat transfer, free-convective turbulent flow, open-ended vertical annuli, radiation shielding*

Introduction

Flexible risers such as flexible pipes and umbilical cables find increasing application in the marine environment and represent a crucial element of a floating production system. This represents an attractive alternative to a rigid riser since a flexible one does not require heavy compensation and tensioning devices at the top or riser manifold at the sea bed. At the same time, it provides ease of installation, retrieval and usage elsewhere. Flexible pipes and umbilical cables both work as composite pipes that are compliant and highly deformable in bending, but strong and stiff in response to internal pressure, external pressure, tension and torque. Umbilical cables generally consist of electrical conductors for signal and power transmissions that are surrounded by a number of protective layers. The protective layer is designed to secure the conductors from adverse chemical and mechanical damage.

One important aspect of the operation of umbilicals is related to their internal temperature. The internal electrical conductor may produce a high amount of heat in case the umbilical is used for electrical power transmission. In order to maintain the integrity and functionality of the umbilicals, the internal temperature should not be higher than around 90°C (363 K) (Bai and Bai, 2010). Usually, the submersed part of the umbilical is adequately cooled by the surrounding seawater. On the other hand, the dry part above the sea level can reach high temperatures, especially if exposed to sun radiation. In order to shield the umbilical cable from sun radiation effects, a stainless steel tube can be placed concentrically to the umbilical's axis, forming an annular space filled with air. The hot surfaces surrounding the open-end concentric annuli create a unique natural convection air flow inside the cavity.

The air flow inside vertical concentric annuli has been investigated by several authors (El-Shaarawi and Al-Nimr, 1990; El-Shaarawi and Negm, 1999; Qi and Shiming, 1999; Takahashi et al., 2001). Most of these works are related to laminar natural convection in open-ended vertical annuli. No prior investigation dealing with the geometry, asymmetries in the boundaries conditions and the conjugated heat transfer problem analyzed in the present work were found in the literature. El-Shaarawi and Al-Nimr (1990) presented analytical solutions for fully developed natural convection in open-ended vertical concentric annuli. The applied fundamental boundary conditions are obtained by combining uniform heat flux or temperature. The influence of the wall-to-fluid thermal conductivity ratio has been investigated and found to have prominent effects on the heat transfer process. The flow regime considered is laminar in steady state condition. No discussion is held about the laminar to turbulent transition. Qi and Shiming (1999) built an experimental apparatus in order to evaluate the convective heat transfer coefficient in vertical annuli over a wide range of Rayleigh Numbers (Ra). In the reported experiments of natural convection in vertical annuli, the inner wall provides a constant heat flux and the cooled outer wall loses heat to the surroundings. Furthermore, the geometry and boundaries conditions were axisymmetric. The influence of the flow regime (laminar, transitional or turbulent) on the convective heat transfer is considered. The authors state that the flow is considered laminar for Ra lower than 4×10^6 and turbulent boundary layer flow is found for Ra greater than 7×10^7. Experimental correlations are presented for different aspect and diameter ratios. El-Shaarawi and Negm (1999) studied the conjugated heat transfer problem in vertical open-ended concentric annuli under laminar flow conditions. The effect of wall heat conduction on natural convection heat transfer is investigated. The solid to fluid thermal conductivity ratio is found to have prominent influence on the induced flow behavior and heat transfer parameters. However, for high values of solid to fluid thermal conductivity ratio, the wall thermal conduction resistance can be neglected.

The objective of this work is to predict the temperature distribution of partially submersed umbilical cables under different operating and environmental conditions. A radiation shield consisting of a partially submersed cylindrical steel tube is also considered, causing a natural convection flow in open-end vertical annuli. The influence of parameters such as the heat dissipating rate, wind velocity, air temperature and solar radiation is analyzed.

Nomenclature

A = *area,* m^2
e = *total specific energy, J/kg*
g = *acceleration of gravity,* m/s^2
G_b = *buoyancy contribution to turbulent kinetic energy,* $kg/(m\ s^3)$

Paper received 24 December 2009. Paper accepted 10 January 2012
Technical Editor: Celso Morooka

G_k = *generation of turbulent kinetic energy due to mean velocity gradient, kg/(m s^3)*
h = *specific enthalpy, J/kg*
$\bar{h}$ = *convection coefficient, W/(m^2 K)*
k = *thermal conductivity, W/(m K)*
k = *turbulent kinetic energy, m^2/s^2*
P = *mean static pressure, Pa*
P_n = *reference hydrostatic pressure, Pa*
$\dot{q}$ = *heat transfer rate, W*
Ra = *Rayleigh Number, dimensionless*
S_e = *volumetric internal energy conversion rate, W/m^3*
S_{ij} = *mean deformation rate tensor, 1/s*
U_i = *mean velocity, m/s*
u' = *velocity fluctuation, m/s*
v = *magnitude of the velocity vector, m/s*
x_i = *spatial coordinate in index notation, m*
y^+ = *normalized wall distance, dimensionless*

Greek Symbols

β = *thermal expansion coefficient, 1/K*
δ_{ij} = *Kronecker unit tensor, dimensionless*
ε = *surface emissivity, dimensionless*
ε = *dissipation rate of the turbulent kinetic energy, m^2/s^3*
ε_{ij} = *dissipation tensor, m^2/s^3*
ν = *kinematic viscosity, m^2/s*
ν_t = *kinematic eddy viscosity, m^2/s*
ρ = *mean specific mass, kg/m^3*
ρ_n = *reference specific mass, kg/m^3*
Θ = *mean temperature, K*
Θ_n = *reference temperature, K*
Θ_∞ = *external fluid temperature, K*
Θ_s = *solid surface temperature, K*
Θ_{rad} = *environment radiative temperature, K*
σ = *Stefan-Boltzmann constant = 5.67 x 10^{-8} W/(m^2 K^4)*
$\tau_{ij}^t = -\overline{u_i' u_j'}$ = *specific Reynolds shear stresses, m^2/s^2*
σ_ε = *turbulent Prandtl number for the dissipation rate of the turbulent kinetic energy, dimensionless*
σ_k = *turbulent Prandtl number for the turbulent kinetic energy, dimensionless*
σ_t = *turbulent Prandtl number for mean total energy, dimensionless*

Problem Description and Geometry

An umbilical cable with 260 mm of external diameter is housed concentrically in a stainless steel tube of 500 mm of external diameter and 25 mm of wall thickness (Fig. 1). The heat generated inside the cable is 55 W/m which corresponds to a volumetric heat generation of 2735 W/m^3. The incident solar radiation on the steel tube (707 W/m^2) was also considered. The temperature of the ambient air is considered to be 40ºC (313 K), windless, which corresponds to the worst possible scenario. The sea water temperature is 25ºC (298 K). The heat generated in its length (7 m) is dissipated by heat transfer to the water for the submersed length (3 m) and also through the natural convection in the annular space between the umbilical surface and internal surface of the steel tube (radiation shield). This steel tube is heated by the sun radiation and cooled by the seawater, as it has 1 m of its length submersed.

The main hypothesis adopted herein is related to the generation and transport of heat inside the umbilical cable. The cross-section geometry of the umbilical cable is complex due to the configuration of the electrical conductors. In order to model the real geometry, four different layers, each one with a constant thermal conductivity, were considered. The following values of the thickness and the thermal conductivity of each layer were considered:

1. External radius of the umbilical cable: 130 mm;
2. Thickness of the 1st layer of the cable (outer layer): 8 mm (k = 0.24 W/(m K));
3. Thickness of the 2nd layer of the cable (shielding): 12 mm (k = 49.8 W/(m K));
4. Thickness of the 3rd layer of the cable (insulation): 30 mm (considered k = 0.3 W/(m K));
5. Thickness of the 4th layer of the cable (inner conductor): 80 mm (considered k = 62 W/(m K)).

The flow in the annular region is governed by the natural convection. Because of the dimensions of the system and to the temperature differences involved, the flow is turbulent. The standard $k-\varepsilon$ turbulence model was chosen for the study because it is suitable for the present case. The following additional hypotheses were adopted for modeling the problem: steady-state; fluid with constant physical properties; and uniform radiative flux on half of the surface of the steel tube.

Figure 1 shows the schematic view and boundary conditions for the problem studied.

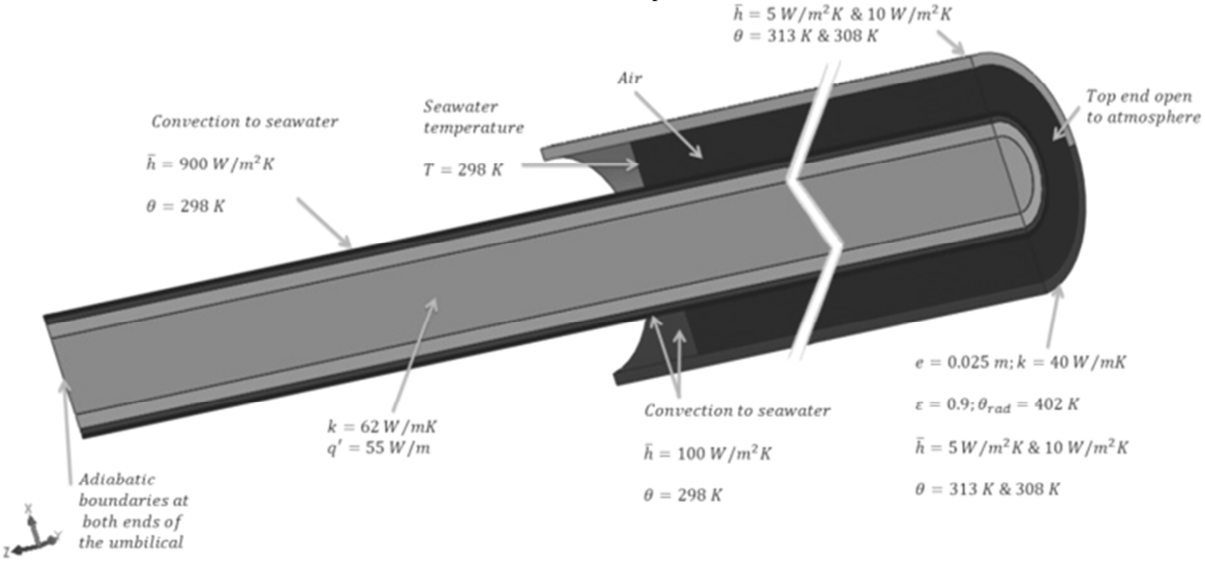

Figure 1. Schematic view (out of scale) and boundary conditions.

Mathematical Formulation

1. Governing Equations

The air flow in the annular region between the umbilical cable and the radiation shield is described by the Navier-Stokes equations. The air movement in the annular region is driven by natural convection effects because of the temperature differences between the air and the surroundings surfaces, i.e. the radiation shield and the riser.

Most of the papers on natural convection inside annuli consider laminar regime for the flow inside the annuli. Qi and Shiming (1999) discuss the influence and quantification of the flow regime. According to that work, a typical Rayleigh Number of the flow studied in the present paper would be about 7 x 10^5, which is in the laminar regime. In the present work, simulations were carried out without turbulence models, but no convergence was achieved. The authors consider, therefore, that such a Rayleigh definition and range do not apply to the present geometry and boundary conditions. This is mainly due to the asymmetries of the cases studied. Based on this reasoning, the flow is considered three-dimensional and in turbulent regime. Additionally, the Boussinesq approximation (Arpaci and Larsen, 1984) is used to account for the density variations only in the buoyancy term.

The Reynolds Averaged Navier Stokes (RANS) equations in Cartesian tensor form read:

$$\frac{\partial U_i}{\partial x_i} = 0 \tag{1}$$

$$\frac{\partial}{\partial x_j}\left(U_i U_j\right) = -\frac{1}{\rho_n}\frac{\partial (P - P_n)}{\partial x_i} + \frac{\partial}{\partial x_j}\left(\nu \frac{\partial U_i}{\partial x_j}\right) + \frac{\partial}{\partial x_j}\left(-\overline{u'_i u'_j}\right) - \left(\frac{\rho - \rho_n}{\rho_n}\right) g_i \tag{2}$$

where U is the mean velocity, u' is the velocity fluctuation, P is the mean pressure, P_n is the reference hydrostatic pressure corresponding to the reference specific mass ρ_n and ν is the molecular kinematic viscosity. g_i is the gravitational acceleration. The specific mass deviation $(\rho - \rho_n)$ is related to the temperature through the following linear equation of state:

$$\frac{\rho - \rho_n}{\rho_n} = -\beta(\Theta - \Theta_n) \tag{3}$$

where Θ is the mean temperature, β is the thermal expansion coefficient and Θ_n is the reference temperature.

The momentum equations include the specific turbulent stress tensor $\tau_{ij}^t = -\overline{u'_i u'_j}$ which is modeled using the standard $k - \varepsilon$ turbulence model, as described below.

The energy equation takes into account the thermal effects, allowing the calculation of the temperature field. The mean total specific energy conservation equation reads:

$$\frac{\partial (U_i(\rho e + P))}{\partial x_i} = \frac{\partial}{\partial x_i}\left(k + \frac{\mu_t}{\sigma_t}\right)\frac{\partial \Theta}{\partial x_i} + S_e \tag{4}$$

where k is the thermal conductivity, σ_t is the turbulent Prandtl Number for the mean total energy and S_e is a volumetric internal energy conversion rate. The mean total specific energy e is defined as

$$e = h - \frac{P}{\rho} + \frac{\nu^2}{2} \tag{5}$$

where h is the specific enthalpy.

For solids, the energy Eq. (4) is reduced to:

$$k\frac{\partial^2 \Theta}{\partial x_i \, \partial x_i} + S_e = 0 \tag{6}$$

Equation (6) applies to the four layers of the umbilical cable as well as to the radiation shield. However, only the 4th layer of the umbilical cable (inner conductor) has the energy source term ($S_e = 2735\ W/m^3$) because of the heat generated inside the cable.

The equations for the momentum balance include the turbulent stress tensor $\tau_{ij}^t = -\overline{u'_i u'_j}$, which is modeled using the $k - \varepsilon$ approach (Launder and Spalding, 1974).

In the $k - \varepsilon$ closure, transport equations for mean turbulent kinetic energy k can be written as:

$$\frac{\partial}{\partial x_j}\left(\rho k U_j\right) = \frac{\partial}{\partial x_j}\left[\left(\mu + \frac{\mu_t}{\sigma_k}\right)\frac{\partial k}{\partial x_j}\right] + G_k + G_b - \rho\varepsilon \tag{7}$$

and for the turbulent kinetic energy dissipation rate ε:

$$\frac{\partial}{\partial x_j}\left(\rho \varepsilon U_j\right) = \frac{\partial}{\partial x_j}\left[\left(\mu + \frac{\mu_t}{\sigma_\varepsilon}\right)\frac{\partial \varepsilon}{\partial x_j}\right] + C_{1\varepsilon}\frac{\varepsilon}{k}(G_k + C_{3\varepsilon}G_b) - C_{2\varepsilon}\rho\frac{\varepsilon}{k} \tag{8}$$

in which $G_k = -\rho\overline{u'_i u'_j}\frac{\partial U_j}{\partial x_i}$ accounts for the generation of turbulent kinetic energy due to the mean velocity gradient. After the Boussinesq hypothesis, G_k is modeled as:

$$G_k = \mu_t S^2 \tag{9}$$

in which S is related to the mean deformation rate tensor by

$$S = \sqrt{2 S_{ij} S_{ij}} \tag{10}$$

The turbulent viscosity μ_t is estimated by

$$\mu_t = \rho C_\mu \frac{k^2}{\varepsilon} \tag{11}$$

The buoyancy contribution to turbulent kinetic energy is given by

$$G_b = \beta g_i \frac{\mu_t}{\sigma_t}\frac{\partial \Theta}{\partial x_i} \tag{12}$$

In order to account for the wall effects on the flow, a specific treatment on the near wall region is used. Depending on the normalized wall distance (y^+), either the laminar or the turbulent model is applied. In the fully turbulent region, $y^+ > 11$, a standard wall function is used for both velocities and energy. Further details concerning near wall treatment can be found in Wilcox (2000) and Fluent (2009). The constants used in Eqs. (6) to (11) are $(C_{1\varepsilon}, C_{2\varepsilon}, C_\mu, \sigma_k, \sigma_\varepsilon) = (1.44, 1.92, 0.09, 1.0, 1.3)$.

The radiative heat transfer between the umbilical and radiation shield was accounted for using the Discrete Ordinates Model. Since the air in the annular region is a non-participating media, a surface to surface radiation model could be used to compute the radiative heat transfer. However, due to the use of symmetry boundary conditions for the flow calculation, the only suitable radiation model in the Fluent solver is the Discrete Ordinates Model. The non-participating media is considered by setting the absorption and scattering coefficient to zero at the Radiative Transport Equation.

2. Boundary Conditions

The convective boundary conditions for the solid material were either adiabatic surface or specified mean convection coefficient $(\bar{h})$ and external fluid temperature (Θ_∞). The heat transfer rate $(\dot{q})$ with specified convection coefficient and fluid temperature can be computed by:

$$\dot{q} = A\bar{h}(\Theta_s - \Theta_\infty) \tag{13}$$

where A is the area of solid surface and Θ_s is its temperature.

For the external surface of the stainless steel tube (the radiation shield), a convective heat transfer coefficient of 5 W/(m^2 K) was prescribed. It corresponds to the lowest possible heat transfer coefficient for natural convection around the radiation shield for the windless conditions. For parametric studies purpose, a convective coefficient of 10 W/(m^2 K) was also considered for a 3 m/s wind velocity. It should be mentioned that higher velocities are possible in the sea environment, but they are less critical as the intention of this paper is to perform critical heat dissipation studies.

The convective heat transfer coefficient for the immersed part of the cable was set to 900 W/(m^2 K), corresponding to a seawater velocity of 0.25 m/s. This was the same value of the convective coefficient for the external surface of the immersed part of the stainless steel tube. The prescribed coefficient for the immersed annular region between the cable and the steel tube was 100 W/(m^2 K). Both seawater convection coefficients are conservative values.

Both the bottom and top end of the solid materials were set up as adiabatic surfaces.

Additionally to the convective heat transfer, the radiation shield receives the solar radiative heat flux. As depicted in Fig. 1, the computational domains encompass just half of the umbilical cable and radiation shield. Therefore, the solar radiative heat flux is imposed only over half of the simulated radiation shield. The incident solar radiation heat flux was assumed to be 707 W/m^2, which leads to an environmental radiant temperature (Θ_{rad}) of 402 K for an averaged solid surface temperature of 363 K. Using the environmental radiant temperature, it is possible to impose the radiative heat power by specifying a temperature (Θ_{rad}) according to

$$\dot{q} = A\varepsilon\sigma\left(\Theta_{rad}^4 - \Theta_s^4\right) \tag{14}$$

The external emissivity of the shell was assumed to be 0.9. The external surface temperature of the radiation shield (Θ_s) is obtained according to the energy balance between convective heat flux, Eq. (13), radiative heat flux, Eq. (14), and heat conduction flux inside the shell, Eq. (6). For all internal surfaces, the emissivity was assumed equal to 1.0.

The boundary conditions for the air in the annular region were no slip wall condition on the surfaces in contact with the solids and seawater and prescribed pressure at the top end of the annular region open to the atmosphere. The bottom end of the annular region was closed by seawater at 25ºC (298 K) so that a temperature of 298 K was prescribed for the air at the bottom end. In order to account for the wall effects on the flow, a specific treatment on the near wall region is used. Depending on the normalized wall distance, either the laminar or the turbulent model is applied. In order to account for the turbulent flow near the wall, the wall-functions method (Launder and Spalding, 1974) is applied for both velocity and temperature.

The above described boundary conditions are depicted in Fig. 1 and summarized in Table 1.

Table 1. Boundary conditions.

Surface	**Boundary conditions**
Bottom and top end of the cable	Adiabatic
Part of the cable immersed in the seawater	$\bar{h}$ = 900 W/m^2; Θ_∞ = 298 K
Part of the external surface of the radiation shield immersed in seawater	$\bar{h}$ = 900 W/m^2; Θ_∞ = 298 K
Part of the cable in the annular region with seawater	$\bar{h}$ = 100 W/m^2; Θ_∞ = 298 K
Left half of the external surface of the radiation shield	$\bar{h}$ = 5 W/m^2; Θ_∞ = 313 K & $\bar{h}$ = 10 W/m^2; Θ_∞ = 308 K No-solar radiative heat flux
Right half of the external surface of the radiation shield	$\bar{h}$ = 5 W/m^2; Θ_∞ = 313 K & $\bar{h}$ = 10 W/m^2; Θ_∞ = 308 K ε = 0.9; Θ_{rad} = 402 K
Air inside the annular region – bottom end	Wall – no slip Θ_∞ = 298 K
Air inside the annular region – top end	Atmospheric pressure – 101 kPa; Θ_∞ = 313 K

3. Numerical Model

The transport equations described above are discretized using the finite volume method (Veersteg and Malalasekera, 2007). All flux terms are approximated by a second order UPWIND discretization scheme on the cell face. The system of algebraic equations is solved by the segregated method where the pressure velocity coupling was conducted by the SIMPLE algorithm. The simulations were carried out using the CFD commercial code Fluent®.

All equations were considered converged when, for each conservation equation, the sum of the normalized residues all over the grid were lower than 10^{-5}. For the energy equation, the residue was lower than 10^{-8}. The numerical grids contained 1 x 10^6 and 6 x 10^6 volumes. The grid independency was checked by performing local refinement on the regions of high velocity gradients. Results from two numerical grids (1 x 10^6 and 6 x 10^6 volumes) were compared and no significant differences on the global velocity and temperature fields were observed.

For the Discrete Ordinates Model, each octant of the angular space 4π at any spatial location is discretized into four solid angles.

Typically, the simulations were carried out through 10000 time-steps, which represent a CPU time of approximately 12 hours using 4 cores on an Intel ® Core i7 2.0GHz processor, with 8 GB RAM.

Results

The simulated cases are presented below. The changed parameters for the four studied cases are summarized in Table 2.

Table 2. Cases studied.

	$\bar{h}$ [W/(m^2 K)]	Θ_∞[K]	Θ_{rad} [K]	S_e [W/m^3]
Case 1	5	313	402	2735
Case 2	5	313	-	2735
Case 3	5	313	402	0
Case 4	10	308	402	2735

The first case corresponds to the base-case, for the worst possible scenario. The second case corresponds to the case in which there are no solar radiation effects. The third case considers null electrical current through the umbilical cable and the temperature rising occurs because of solar radiation only. The fourth case takes into account a lower air temperature (35ºC = 308 K) and a higher convective coefficient (h = 10 W/(m^2 K)), which is somewhat closer to the actual sea environmental conditions.

The air velocity distribution for case 1 is presented in Fig. 2. The air velocities at the bottom horizontal plane and symmetry plane (Fig. 2a) and at the top horizontal plane (Fig. 2b) of the annular region are shown. The velocity vectors are the interpolated values at the center of the first control volume inside the grid. The complex 3D flow inside the annular region between the umbilical cable and the radiation shield can be observed in Fig. 2a.

At the top horizontal plane (Fig. 2b), one can see the outward velocities on the side of higher temperatures (right) at the radiation shield and the inward velocities on the opposite side. Similar velocity distributions were obtained for the other studied cases and are not shown here.

Figure 2c indicates the axial velocity profile at the vertical symmetry plane. On the positive side of the transverse position of the symmetry plane, the air moves upward because of the buoyancy effect of the heated surfaces, both the cable and the radiation shield. The opposite side shows the air going downward because of the continuity effect, although the cable is heated. The velocity profiles in other axial positions and vertical planes indicate that the flow is very complex, non-uniform and includes a tangential component.

The temperature distribution for each simulated case is presented in Figs. 3 to 5.

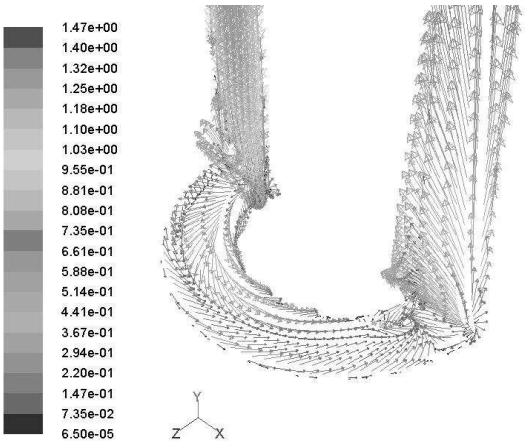

Figure 2a. Case 1 – Air velocity distribution at the horizontal bottom plane and symmetry plane.

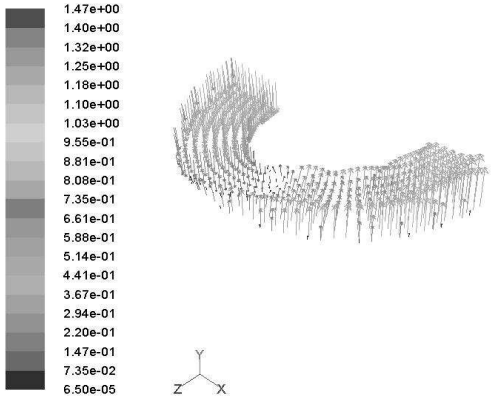

Figure 2b. Case 1 – Air velocity distribution at the horizontal top plane.

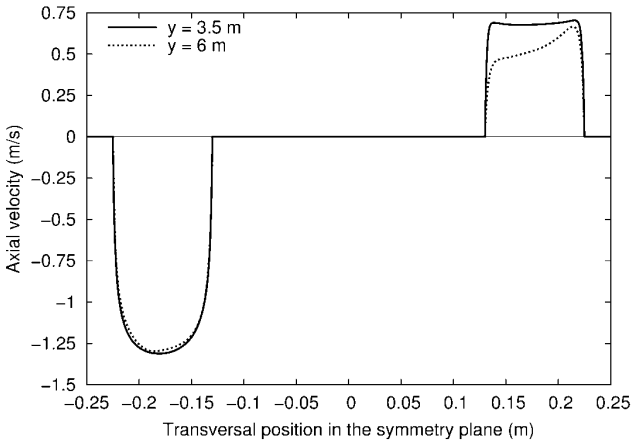

Figure 2c. Case 1 – Air axial velocity (m/s) at cut plane y = 3.5 and 6.0 m.

Figure 3a displays, on the left part, the temperature distribution (K) at the symmetry plane for case 1. The maximum temperature in this plane (Θ_{max} = 360 K) is in the radiation shield. In the umbilical cable, the maximum temperature (357 K) is in its central part, where there is heat generation and where the cooling effects by the air (upper region) and by the seawater (bottom region) are smaller. The right side, slightly hotter, receives the solar radiation flux. For this case, the total heat lost to the air was 214.3 W (55.4%) and to the water was 172.2 W (44.6%). It is worth noting that the amount of heat lost through the submersed cable, and also through the submersed steel tube, is significant. The heat transfer in the radiation shield towards the seawater can be inferred by observing the longitudinal temperature gradients in Figs. 3a and 3b. The latter also displays the temperature distribution on the surface of the umbilical cable. The maximum cable surface temperature (354 K) also occurs in the region of the cable where the heating effect of solar radiation is maximum and the cooling effect of the extremities is minimum. The temperature distribution on the radiation shield surface is shown on the right part of Fig. 3a. It is easy to see the influence of solar radiation on the steel shield. It is worth emphasizing that, for the simulated domain – one half of the umbilical cable and steel shield – the boundary conditions, concerning the steel shield, are solar radiation combined with convection over one half and solely convection over the other half of the shield. From the results shown in Fig. 3b, one can conclude that although there is a significant asymmetry in the air temperature, the temperature of the innermost cable layer is almost symmetric.

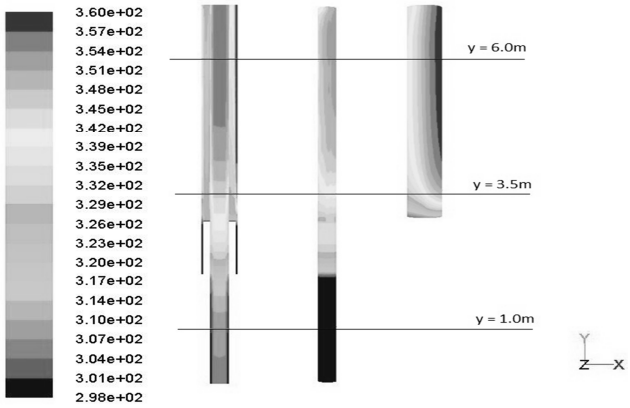

Figure 3a. Case 1 – Temperature distribution (K) in the symmetry plane, cable surface and radiation shield.

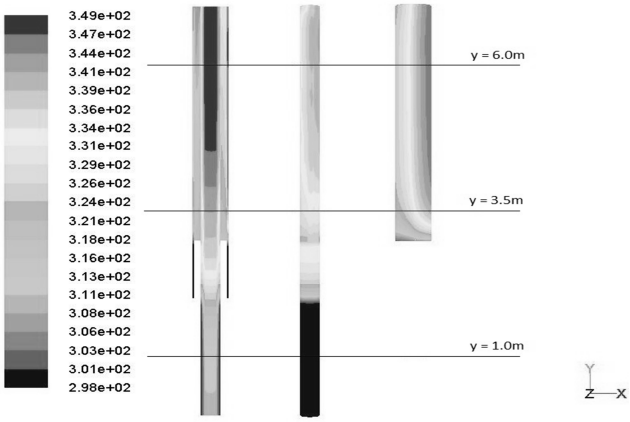

Figure 5a. Case 4 – Temperature distribution (K) in the symmetry plane, cable surface and radiation shield.

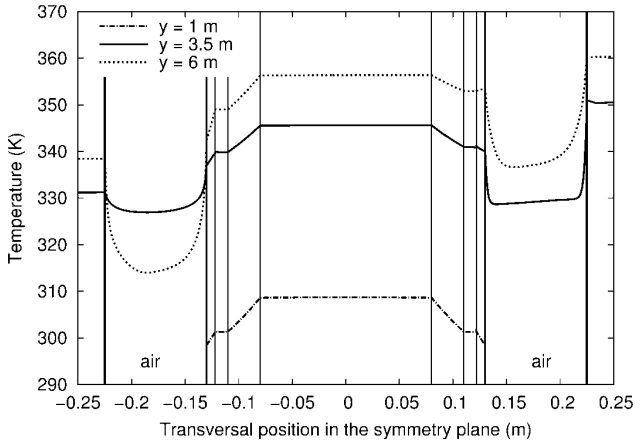

Figure 3b. Case 2 – Temperature distribution (K) in the symmetry plane, cable, air and radiation shield at cut plane y = 1.0, 3.5 and 6.0 m. Vertical lines depict the interfaces air/solid or solid/solid.

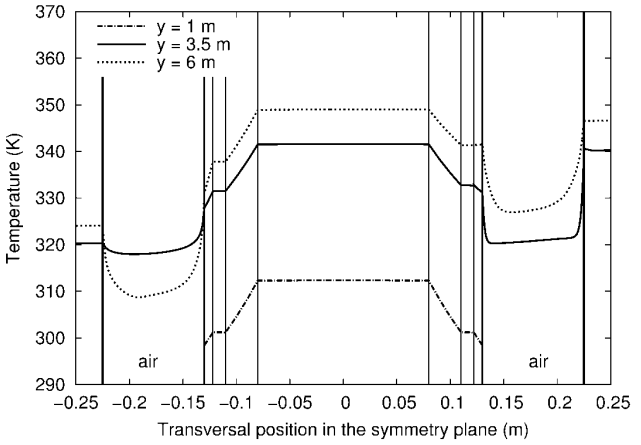

Figure 5b. Case 4 – Temperature distribution (K) in the symmetry plane, cable, air and radiation shield at cut plane y = 1.0, 3.5 and 6.0 m. Vertical lines depict the interfaces air/solid or solid/solid.

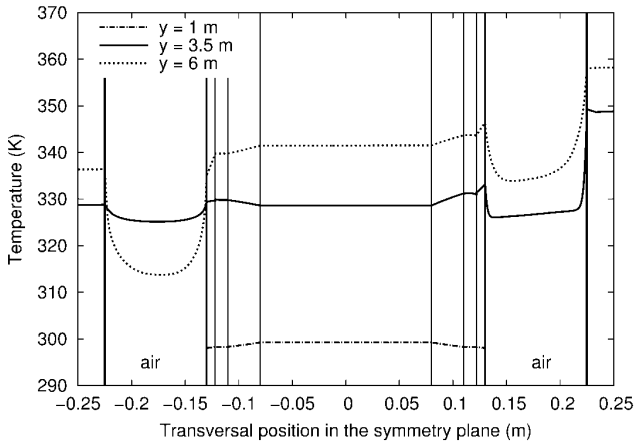

Figure 4. Case 3 – Temperature distribution (K) in the symmetry plane, cable, air and radiation shield at cut plane y = 1.0, 3.5 and 6.0 m. Vertical lines depict the interfaces air/solid or solid/solid.

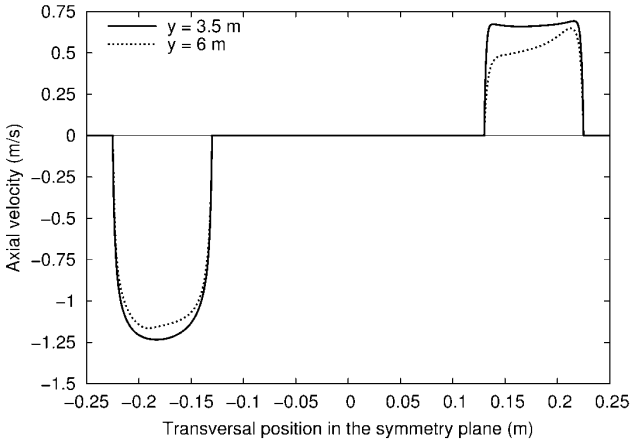

Figure 5c. Case 4 – Air axial velocity (m/s) at cut plane y = 3.5 and 6.0 m.

In case 2, the effect of the absence of solar radiation on the heat transfer in the umbilical cable was studied. The maximum temperature in the symmetry plane ($\Theta_{max} = 332$ K) decreases significantly when compared to case 1, with solar radiation of 707 W/m^2 ($\Theta_{max} = 357$ K). The total heat lost to the air was 227.2 W (59.2%) and to the water it was 156.8 W (40.8%). The absence of solar radiation increases the amount of heat loss in the dry part of the cable because of the lower air temperatures in the annular region. The maximum cable surface temperature in this case is 326 K.

In case 3, the effect of the absence of heat generated by the Joule effect in the umbilical cable was studied. The purpose of simulating this case was to evaluate the radiation influence alone. The temperature distribution for this case is shown in Fig. 4.

The maximum temperature ($\Theta_{max} = 358$ K) happens in the external wall of the steel tube that receives solar radiation. In fact, the heating of the umbilical cable is produced by the effect of solar radiation and of the high temperature of the ambient air considered in the simulation ($\Theta_{\infty} = 313$ K). The heat received (26.2 W) in the dry part of the cable, by natural convection and radiation, is conducted by the cable to the bottom part and lost by convection to the seawater. On the positive part of the symmetry plane, one can see the influence of the two heat transfer modes. The cable is heated by radiation whereas the air cools it.

As the air temperature and its convective coefficient have a significant effect on the simulation results, and considering that the values used in the previous cases were too conservative (worst possible scenario), a new set of more realistic values for these parameters were simulated in case 4. An air temperature of 308 K and a convective coefficient of 10 W/(m^2 K) were considered, which corresponds to a breeze with speed lower than 3 m/s. Figure 5a displays the temperature distribution in the symmetry plane for this case. The maximum temperature ($\Theta_{max} = 349$ K) is slightly lower than in case 1 ($\Theta_{max} = 357$ K), as is the maximum cable surface temperature (344 K). The major difference between cases 1 and 4 can be verified at the temperature distribution on the steel shield. Comparing Figs. 3b and 5b, the maximum steel shield temperature ($\Theta_{max} = 349$ K) for case 4 is observed to be significantly lower than for case 1 ($\Theta_{max} = 360$ K). The external heat transfer conditions have a more pronounced impact on the steel shield temperature. In turn, the flow velocity field is affected by the higher heat transfer coefficient and lower air temperature, as shown in Fig. 5c. Comparing Fig. 5c with Fig. 2c, the downwash velocity (left side) in cut plane y = 6 m for case 4 is observed to be weaker (approximately 0.15 m/s) than for case 1.

Table 3. Energy balance and maximum temperatures for the cases studied.

	Case 1	Case 2	Case 3	Case 4
Heat transfer – dry part (W)	-214.3	-227.2	26.2	222.6
Heat transfer – wet part (W)	-172.2	-156.8	-26.9	164.3
Relative energy imbalance (%)	0.4 *	0.2 *	0.03 **	0.5 *
Maximum cable surface temperature (K)	354	326	349	344
Maximum cable temperature (K)	357	332	349	349

* Referred to the internally generated heat – 385 W

** Referred to the solar radiation flux of 707 W/m^2 over half of the radiation shield – 2221 W

The energy balance in the umbilical cable summarized in Table 3 shows the heat transfer rates from the cable to the environment in the dry part (4 m of length) and in the wet part (3 m of length) of the cable. The maximum cable temperature and the cable surface temperature are also presented. From the results presented in Table 3, one can see that the energy balance is satisfied in all the simulated cases. This is a further validation of the proposed model. Case 1 corresponds to the most severe environmental conditions (windless, air temperature of 313 K and maximum solar radiation). In this case, the maximum temperature inside the cable, generating 55 W/m of heat, is 357 K. This value is close to the maximum allowable temperature inside the umbilical, which is 363 K. For less severe environmental conditions (breeze of 3 m/s and air temperature of 308 K), corresponding to case 4, the maximum temperature is 349 K, which is 8 K lower than that in case 1. This sensitivity analysis shows that small changes in the environmental conditions produce a variation in the maximum temperature which allows the umbilical to work under a less critical condition. It is important to note that these simulations were conducted for the worst possible scenario. In both cases, a solar radiation flux of 707 W/m^2, which is a high value for the radiation, was considered. In case 2, the absence of solar radiation causes a substantial decrease (25 K) in the cable temperatures because of the decrease of the steel tube temperature. In case 3, the absence of internal heat generation also results in a significant decrease of the innermost cable temperatures (341 K). It means that solar radiation has a smaller effect on the maximum temperature of the cable than the heat generated by the Joule effect, at least for the parameters set imposed in the present study. The results of the numerical simulation also indicate that the seawater cooling of the umbilical cable and of the steel tube is an important heat transfer mechanism.

Conclusions

The objective of predicting the temperature distribution of partially submersed umbilical cables under different operating and environmental conditions was successfully attained. The Fluent® code was used to simulate the heat transfer and air fluid flow of part of a vertical umbilical cable near the air-water interface. A free-convective three-dimensional turbulent flow in open-ended vertical annuli was solved. The influence of parameters such as the

heat dissipating rate, wind velocity, air temperature and solar radiation was analyzed. The proposed model was deemed validated by considering grid independence, reproduction of symmetric boundary conditions and the overall energy balance. The results indicate that the influence of a hot environment and intense solar radiation may affect the umbilical cable performance in its dry portion. For the most severe environmental conditions (windless, air temperature of 313 K and maximum solar radiation), the maximum temperature inside the cable was 357 K. For less severe environmental conditions (breeze of 3 m/s and air temperature of 308 K), the maximum temperature was 349 K. These results show that small changes in the environmental conditions may produce considerable decreases of maximum temperature in the umbilical. The major difference between these two cases was observed at the external temperature of the radiation shield. The absence of solar radiation or the internal heat generation cause a substantial decrease in the cable temperatures. The results of the numerical simulations also indicate that heat transfer from the umbilical cable and from the steel tube to seawater is an important cooling mechanism.

Acknowledgement

The authors would like to thank Mr. Newton K. Fumukasu for preparing the numerical meshes.

References

Arpaci, V.S. and Larsen, P.S., 1984, "Convection Heat Transfer", Prentice-Hall, Englewood Cliffs, NJ.

Bai, Y. and Bai, Q., 2010, "Subsea Umbilical Systems" in "Subsea Structural Engineering Handbook", Gulf Professional Publishing, Boston, MA, pp. 797-825.

El-Shaarawi, M.A.I. and Al-Nimr, M.A., 1990, "Fully developed laminar natural convection in open-ended vertical concentric annuli", *International Journal of Heat and Mass Transfer*, Vol. 33, pp. 1873-1884.

El-Shaarawi, M.A.I. and Negm, A.A.A., 1999, "Conjugated natural convection heat transfer in an open-ended vertical concentric annuli", *Numerical Heat Transfer – Part A*, Vol. 36, pp. 639-655.

Fluent User's Guide, 2009, http://www.fluentusers.com/

Launder, B.E. and Spalding, D.B., 1974, "The numerical computation of turbulent flows", *Computer Methods in App. Mech. and Engineering*, Vol. 3, pp. 269-289.

Qi, W. and Shiming, Y., 1999, "Experimental study of natural convection heat transfer of air layers in vertical annuli under high Rayleigh number conditions", *Heat Transfer – Asian Research*, Vol. 28, pp. 50-57.

Takahashi, K., Morikawa, T., Harada, Y. and Hattori, N., 2001, "Natural convective heat transfer in uniformly heated vertical pipe annuli", *Heat Transfer – Asian Research*, Vol. 30, pp. 676-688.

Versteeg, H.K. and Malalasekera, W., 2007, "An Introduction to Computational Fluid Dynamics – The Finite Volume Method", Pearson Prentice Hall, London.

Wilcox, D.C., 2000, "Turbulence Modeling for CFD", DCW Industries, La Cañada, CA.